Journal of Catalysis 257 (2008) 356–368

Contents lists available at ScienceDirect

Journal of Catalysis

www.elsevier.com/locate/jcat

Steam reforming, partial oxidation, and oxidative steam reforming of ethanol over $Pt/CeZrO_2$ catalyst

Sania M. de Lima [a], Ivna O. da Cruz [a], Gary Jacobs [b], Burtron H. Davis [b], Lisiane V. Mattos [a], Fábio B. Noronha [a,*]

[a] Instituto Nacional de Tecnologia - INT, Av. Venezuela 82, CEP 20081-312, Rio de Janeiro, Brazil
[b] Center for Applied Energy Research, The University of Kentucky, 2540 Research Park Drive, Lexington, KY 40511, USA

ARTICLE INFO

Article history:
Received 19 February 2008
Revised 13 May 2008
Accepted 15 May 2008
Available online 20 June 2008

Keywords:
Fuel cell
Hydrogen production
Steam reforming of ethanol
Partial oxidation of ethanol
Oxidative steam reforming of ethanol and $Pt/CeZrO_2$ catalyst

ABSTRACT

The catalytic performance of a $Pt/CeZrO_2$ catalyst was tested for ethanol decomposition, steam reforming, partial oxidation, and oxidative steam reforming. At low temperature, the catalyst underwent significant deactivation during ethanol decomposition and steam reforming reactions. Co-feeding oxygen decreased the deactivation rate of the catalyst but adversely affected the selectivity to hydrogen. Increasing the reaction temperature greatly improved the stability of the catalyst. A reaction mechanism was proposed based on results obtained from in situ diffuse reflectance infrared spectroscopy analyses carried out under reaction conditions. Ethanol adsorbs as ethoxy species, which may follow one of two distinct pathways: (i) decomposition and production of CO, CH_4, and H_2 or (ii) dehydrogenation to acetaldehyde and acetyl species. The dehydrogenated species may undergo oxidation to acetate species. The addition of water to the feed promoted the formation of acetate species. Water also facilitated the decomposition of acetaldehyde and acetate reactions, resulting in the formation of methane, CO, and carbonate.

1. Introduction

The electrochemical conversion of hydrogen to power via polymer electrolyte membrane (PEM) fuel cell technology may alleviate global dependence on fossil fuels, as well as decrease emissions of greenhouse gases and other atmospheric pollutants [1]. Recently, ethanol has been claimed to be an alternative source of hydrogen production for fuel cells, because it can be manufactured from biomass and does not contribute to net CO_2 emissions. The United States, Brazil, and other countries have established an ethanol production and distribution infrastructure.

Hydrogen may be generated from ethanol by different technologies, including steam reforming (SR) (reaction (1)), partial oxidation (POX) (reaction (2)), and oxidative steam reforming (OSR) (reaction (3)) [2]:

$$C_2H_5OH + 3H_2O \rightarrow 2CO_2 + 6H_2, \quad \Delta H_{298} = 347.4 \text{ kJ/mol}, \quad (1)$$

$$C_2H_5OH + 1.5O_2 \rightarrow 2CO_2 + 3H_2, \quad \Delta H_{298} = -554.0 \text{ kJ/mol}, \quad (2)$$

$$C_2H_5OH + 2H_2O + 0.5O_2 \rightarrow 2CO_2 + 5H_2, \quad \Delta H_{298} = -50 \text{ kJ/mol}. \quad (3)$$

All of these reactions have one major drawback, however. Various reaction pathways may operate depending on the conditions selected and the choice of the catalyst. The reaction network may include (i) ethanol decomposition to methane, CO and hydrogen; (ii) ethanol dehydrogenation to acetaldehyde; (iii) ethanol dehydration to ethylene; (iv) methane steam reforming; (v) the water–gas shift reaction; (vi) methane decomposition to carbon and hydrogen; and (vii) the Boudouard carbon deposition reaction [3–5]. A wide range of undesirable byproducts, such as oxygenated compounds (acetaldehyde, acetone) and hydrocarbons like methane and ethane, are formed at low reaction temperatures. Some of these reactions lead to the formation of coke, which can in turn induce catalyst deactivation. At high reaction temperatures, CO production is thermodynamically favored, which, if left unconverted, will poison the electrodes of the PEM fuel cell. Therefore, further purification steps are required, which increases not only the final cost of the hydrogen produced, but also the size and the weight of the fuel processor.

The nature of the metal and support strongly affects the stability and product distribution [3,4]. $CeZrO_2$ has been proposed as a support for the ethanol conversion reactions due to its high oxygen storage capacity (OSC), which improves catalyst stability. In addition, the strong metal–support interaction prevents metal particle sintering, which also contributes to catalyst deactivation [6,7]. Romero-Sarria et al. [7] reported that the use of a catalytic system based on Ce–Zr mixed oxides doped with Co, Ni, Rh, Rh–Co, or Rh–Ni reduced the formation of carbonaceous deposits during SR. In addition, other authors [8,9] have observed that ceria/zirconia-supported metal catalysts exhibit higher H_2 yield than other supports during SR. Recently, we investigated the performance of supported Pt catalysts for POX [10] and SR [11]. The $Pt/CeZrO_2$ catalyst exhibited good activity and stability for POX, which was attributed

* Corresponding author. Fax: +55 21 2123 1051.
E-mail address: fabiobel@int.gov.br (F.B. Noronha).

0021-9517/$ – see front matter
doi:10.1016/j.jcat.2008.05.017

to the material's high OSC [10]. It also exhibited good selectivity to H_2 during SR [11]. Furthermore, a comparison between the results obtained for the $Pt/CeZrO_2$ and Pt/CeO_2 catalysts in SR showed that adding Zr to ceria improved the stability and decreased the CO selectivity of the Pt/CeO_2 catalyst.

Designing an optimum catalyst for hydrogen production from ethanol requires additional insight into the reaction mechanism. The literature contains some studies of the reaction mechanism of ethanol over different catalysts. Most of the ethanol reaction mechanisms proposed in the literature relied on infrared spectroscopy (IR) results that were not measured under steady state conditions. Alternatively, temperature-programmed desorption (TPD) of adsorbed ethanol or ethanol + water mixture was employed. At each temperature of interest, the system was evacuated to determine the adsorbed species present on the catalyst surface [5,12–19].

In a previous investigation by some of us [20], a transient diffuse reflectance infrared spectroscopy (DRIFTS) technique was used to study the activation/turnover of probe molecules of ROH type to gain insight into the low-temperature water–gas shift mechanism under H_2 cofeeding conditions. In that context, CO (from the low-temperature shift) was replaced by ethanol, which was used as a probe molecule to demonstrate two important points: (i) Under conditions of H_2 cofeeding, the activation of ROH molecules is dissociative and common in the water–gas shift, methanol SR, and ethanol SR reactions, and (ii) at least under conditions of H_2 cofeeding and a high H_2O/reactant ratio (reactant = CO, CH_3OH, or C_2H_5OH), formate or acetate plays an important role as an intermediate in these three reactions. Formate, produced from the reaction of CO with –OH during a low-temperature shift or from the conversion of methoxy during methanol SR, is dehydrogenated, and, in an analogous manner, acetate produced from conversion of ethoxy species is demethanated during ethanol SR. In fact, methanol and ethanol were used as probe molecules to shed light on the water–gas shift mechanism, which requires a H_2 cofeed.

These studies were not carried out under reaction conditions by flowing the reaction mixture at different temperatures, however. The nature of intermediate species formed on the surface may be strongly affected by the reaction conditions.

The present study was conducted to investigate the reaction mechanisms for SR, POX, and OSR under realistic stoichiometric feed ratios over the $Pt/CeZrO_2$ catalyst system. The reaction mechanisms were investigated using DRIFTS carried out under steady-state reaction conditions using appropriate feed conditions to mimic ED, SR, and POX. In particular, the effect of oxygen and water on the nature and populations of surface species were assessed.

2. Experimental

2.1. Catalyst preparation

The $CeZrO_2$ support (Ce/Zr ratio = 3) was obtained by the precipitation method as described by Hori et al. [19]. The choice of Ce/Zr ratio was based on findings of our previous study [11] showing that the $Pt/CeZrO_2$ catalyst containing the Ce/Zr ratio of 3.0 exhibited good performance during SR. An aqueous solution of cerium(IV) ammonium nitrate and zirconyl nitrate (Aldrich). Then the ceria and zirconium hydroxides were coprecipitated by the addition of an excess of ammonium hydroxide. Finally, the precipitate was washed with distilled water and calcined at 1073 K for 1 h in a muffle furnace. Platinum was added to $CeZrO_2$ support by the incipient wetness impregnation technique using an aqueous solution of $H_2PtCl_6{\cdot}6H_2O$. After impregnation of 1.5 wt% of platinum, the samples were dried at 393 K and calcined under air (50 mL/min) at 673 K for 2 h.

2.2. BET surface area

The BET surface areas of the samples were measured using a Micromeritics ASAP 2000 analyzer by nitrogen adsorption at the boiling temperature of liquid nitrogen.

2.3. OSC

OSC measurements were carried out in a microreactor coupled to a Balzers Omnistar quadrupole mass spectrometer. Before OSC analysis, the samples were reduced under flowing H_2 at 773 K for 1 h, then cooled to 723 K, and kept at this temperature during the analysis. The mass spectrometer was used to measure the composition of the reactor effluent as a function of time while a 5% O_2/He mixture was passed through the catalyst. Oxygen consumption was calculated from the curve corresponding to $m/e = 32$.

2.4. Cyclohexane (CH) dehydrogenation

Platinum dispersion was estimated by running a reaction to probe the metallic function. CH dehydrogenation was selected, because it is considered a rather structurally insensitive reaction [21]. Because H_2 and CO spillover occurs from the metal to the CeO_2, metal dispersion could not be determined from chemisorption of either gas [22]. Therefore, to provide an estimate of the dispersion of the $Pt/CeZrO_2$ catalyst, a correlation between the rate of CH dehydrogenation and the metal dispersion measured by hydrogen chemisorption was established. The reference catalysts for this procedure were Pt/Al_2O_3 catalysts of varying metal particle size.

CH dehydrogenation was performed in a fixed-bed reactor at atmospheric pressure. The catalyst was reduced at 773 K for 1 h, and the reaction was carried out at 543 K and WHSV = 170 h^{-1}. The reactants were fed to the reactor by bubbling H_2 through a saturator containing cyclohexane to obtain the desired H_2/CH ratio (13:1). The exit gases were analyzed using a Varian 300 gas chromatograph equipped with a HP-INNOWAX column.

2.5. TPD of ethanol

TPD experiments of adsorbed ethanol were carried out in the same equipment described previously for OSC measurements. Before TPD analyses, the samples were reduced under flowing H_2 (30 mL/min) by ramping to 773 K (10 K/min), and holding at this temperature for 1 h. After reduction, the system was purged with helium at 773 K for 30 min and cooled to room temperature. The adsorption of ethanol was carried out at room temperature using an ethanol/He mixture, which was obtained by flowing He through a saturator containing ethanol at 298 K. After adsorption, the catalyst was heated at 20 K/min to 773 K under flowing helium (60 mL/min). The products were monitored using a quadrupole mass spectrometer.

2.6. DRIFTS

DRIFTS spectra were recorded using a Nicolet Nexus 870 spectrometer equipped with a DTGS-TEC detector. A Thermo Spectra-Tech cell capable of high-pressure/high-temperature operation and fitted with ZnSe windows served as the reaction chamber for in-situ adsorption and reaction measurements. Scans were obtained at a resolution of 4 to give a data spacing of 1.928 cm^{-1}. Depending on the signal-to-noise ratio, the number of scans ranged from 256 to 1024. The amount of catalyst was ~40 mg.

Samples were first reduced by ramping in 200 mL/min H_2:He (1:1) at ~10 K/min and holding at 773 K for 1 h. The catalyst was purged in flowing He at 773 K before being cooled in flowing He to 313 K.

For ethanol adsorption, TPD, and temperature-programmed surface reaction (TPSR) (i.e., ethanol decomposition (ED) or SR) tests, He was bubbled through a saturator filled with ethanol and held at 273 K at ∼15 mL/min. For ethanol SR tests, a second helium stream (∼15 mL/min) was bubbled through a saturator filled with water and held at 298 K. The two streams were joined at a T-junction, before which 1-psig check valves were placed on the lines to prevent a backflow condition. The saturator gas flows and temperatures were set to provide a H_2O:CH_3CH_2OH ratio of 2:1, which is nominal for SR. Adsorption/reaction measurements were started at 313 K, and then the temperature was increased at a rate of 10 K/min; measurements were recorded at 373, 473, 573, 673, and 773 K.

2.7. Temperature-programmed oxidation (TPO)

TPO was carried out after 6 h TOS of reaction over Pt/$CeZrO_2$ catalyst to study the nature of the catalyst deactivation. The analysis was performed in the same apparatus described previously for OSC and TPD measurements. After reaction, the catalyst was cooled to room temperature under He, then heated at a rate of 10 K/min to 1273 K under a mixture containing 8% O_2 in He. The products were monitored using a quadrupole mass spectrometer.

2.8. Reaction conditions

ED (i.e., H_2O/ethanol molar ratio = 0.0), SR, POX, and OSR were performed in a fixed-bed reactor at atmospheric pressure. Before the reactions, the catalysts were reduced at 773 K for 1 h and then purged under N_2 at the same temperature for 30 min. All reactions were carried out at 773 K. In addition, SR was performed at 1073 K. POX was conducted using an O_2/ethanol molar ratio of 0.5. The choice of O_2/ethanol ratio was based on the work of Cavallaro et al. [23], who found an ethanol conversion of ca. 100% and H_2 production near maximum when using an O_2/ethanol ratio of 0.4–0.5. For SR, H_2O/ethanol molar ratios of 2.0, 3.0, or 5.0 were used. OSR was performed using a H_2O/ethanol molar ratio of 2.0 and an O_2/ethanol molar ratio of 0.5. SR, POX, and OSR also were carried out without catalyst (homogeneous reaction) at 773 K. The reactant mixtures were obtained using two saturators containing water and ethanol, which were maintained at the temperature necessary to obtain the desired H_2O/ethanol and O_2/ethanol molar ratios. For ED and POX, N_2 (30 mL/min) and a 5.6% O_2/N_2 mixture (30 mL/min), respectively, were passed through the saturator with ethanol, and the resulting reactant mixtures were diluted with N_2 (30 mL/min). For SR, the reactant mixture was obtained by flowing two N_2 streams (30 mL/min) through each saturator containing ethanol and water separately. For OSR, a flow of 5.6% O_2/N_2 (30 mL/min) and a flow of N_2 (30 mL/min) were passed through the saturators containing ethanol and water, respectively. The partial pressure of ethanol was kept constant for all experiments. The variation of partial pressure of water was compensated by the decrease of partial pressure of N_2.

To evaluate the catalyst deactivation within a short time period, a small amount of catalyst was used (20 mg). The samples were diluted with inert SiC (SiC mass/catalyst mass = 3.0). The reaction products were analyzed by gas chromatography (Micro GC Agilent 3000 A) containing two channels for dual thermal conductivity detectors (TCDs) and two columns: a molecular sieve and a Poraplot U column. The ethanol conversion and the selectivity to the products were determined from

$$X_{\text{ethanol}} = \frac{(n_{\text{ethanol}})_{\text{fed}} - (n_{\text{ethanol}})_{\text{exit}}}{(n_{\text{ethanol}})_{\text{fed}}} \times 100 \quad (4)$$

and

$$S_{\text{x}} = \frac{(n_{\text{x}})_{\text{produced}}}{(n_{\text{total}})_{\text{produced}}} \times 100, \quad (5)$$

where $(n_{\text{x}})_{\text{produced}}$ = mol of x produced (x = hydrogen, CO, CO_2, methane, acetaldehyde, or ethene) and $(n_{\text{total}})_{\text{produced}}$ = mol of H_2 + mol of CO + mol of CO_2 + mol of acetaldehyde + mol of ethene (the moles of water produced are not included).

3. Results and discussion

3.1. Catalyst characterization

The BET surface area of $CeZrO_2$ support was very low (34 m^2/g) and was not measurably affected by the addition of platinum. Pt/$CeZrO_2$ catalyst exhibited high oxygen consumption during OSC analysis (626 μmol/g_{cat}). The high OSC of Pt/$CeZrO_2$ can be attributed to the high oxygen mobility of the $Ce_{0.75}Zr_{0.25}O_2$ solid solution formed. XRD data revealed the formation of a CeO_2–ZrO_2 solid solution with a cubic symmetry [24]. Fally et al. [25] obtained similar findings for OSC analysis over $CeZrO_2$ systems. Indeed, ^{16}O–^{18}O switching investigations [26] determined that whereas low-temperature oxygen mobility is confined to the surface shell in pure ceria, considerable oxygen transport between the bulk and surface shell regions occurs over the ceria–zirconia mixed-oxide system. The higher oxygen mobility of the mixed oxide also has been linked to higher extents of reduction over ceria alone [27].

The platinum dispersion of Pt/$CeZrO_2$ catalyst calculated by the CH dehydrogenation probe reaction was relatively low (∼22%). This is likely attributed to the inability of the $CeZrO_2$ support, which exhibited a low BET surface area, to stabilize Pt of small particle size.

3.2. Reactions

A series of hydrogen production test reactions was carried out over the Pt/$CeZrO_2$ catalyst to evaluate the response of the catalyst to different environments, as well as to assess catalyst performance parameters such as conversion, selectivity, and stability. The reactions were investigated at 773 K, including ED, SR, POX, and OSR of ethanol; the main results are summarized in Fig. 1. Comparing the values of initial ethanol conversion obtained for the ED and SR reactions indicate that adding water to the feed increased the initial conversion level. The initial ethanol conversions were similar during the POX and OSR reactions (Figs. 1c and 1d, respectively) and higher than the conversion levels observed for the ED and SR reactions (Figs. 1a and 1b). Kugai et al. [28] also observed that the addition of water and oxygen over Ni–Rh/CeO_2 catalyst increased the ethanol conversion for ED, SR, POX, and OSR.

Ethanol conversion decreased significantly at the beginning of the ED and SR reaction tests, but in both cases, the catalyst became practically stable after 4 h time on stream (TOS). Some authors [29] also observed a strong deactivation for the Rh/CeO_2–ZrO_2 catalysts during SR, which they attributed to carbon deposition on the catalyst surface. Recently, we studied the performance of Pt/CeO_2 and Pt/$Ce_{0.75}Zr_{0.25}O_2$ during the SR of ethanol [11]. The addition of Zr to ceria improved the stability and decreased the CO selectivity of the Pt/CeO_2 catalyst. Despite the slight deactivation observed for both the POX and OSR reactions, from the standpoint of ethanol conversion, adding O_2 to the feed improved catalyst stability. In line with these results, Fierro et al. [30] reported that the introduction of more oxygen increased the stability of Ni–Cu/SiO_2 catalysts during OSR.

The selectivity to hydrogen decreased during the first 3 h TOS for both the ED and SR reactions. After that interval, hydrogen was no longer detected during ED, whereas its selectivity remained relatively stable during SR. For POX, hydrogen formation was very low and was no longer observed after 1 h TOS. The catalyst produced large quantities of H_2 for the first 3 h TOS during OSR, but hydrogen selectivity decreased significantly after this period.

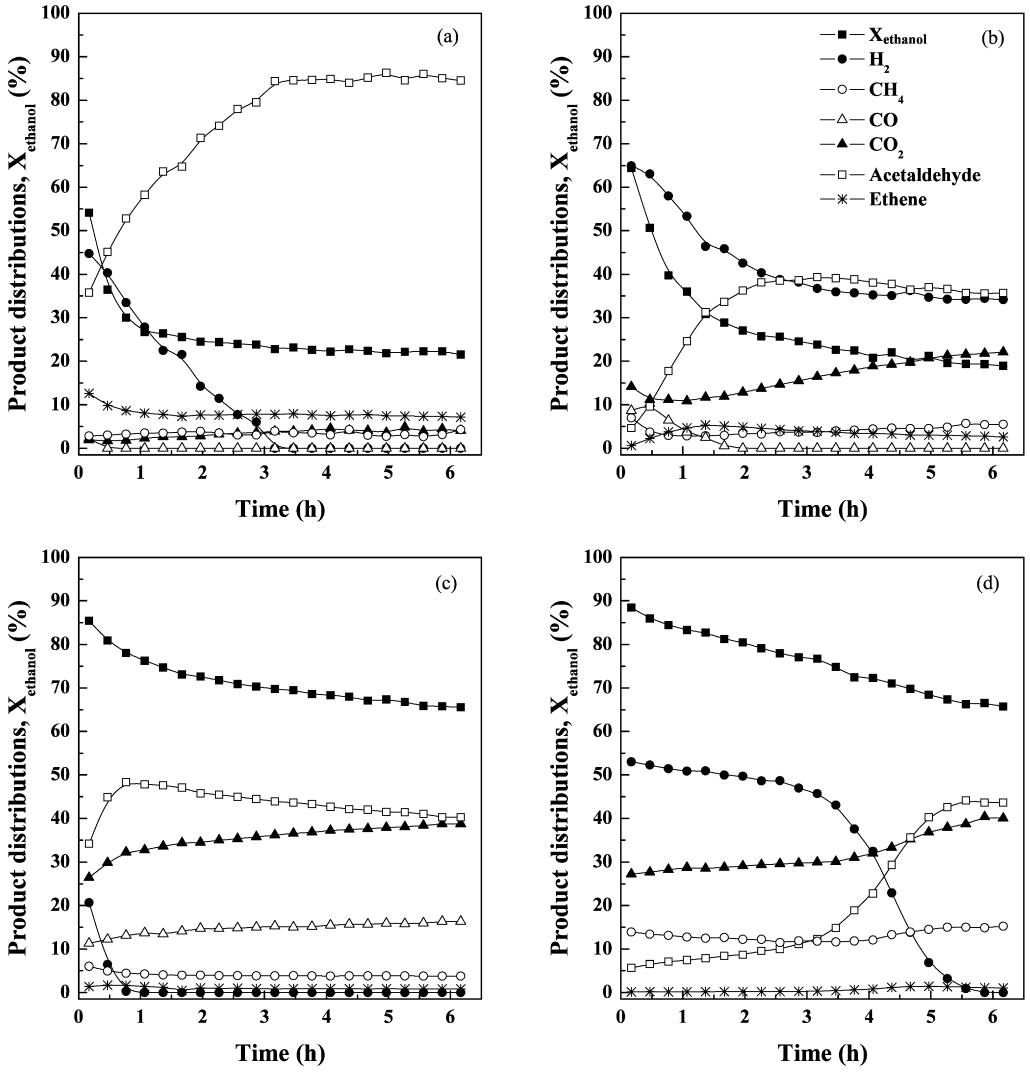

Fig. 1. Ethanol conversion ($X_{ethanol}$) and product distributions versus time on stream obtained during (a) ED, (b) SR, (c) POX and (d) OSR for $Pt/CeZrO_2$ catalyst ($T_{reaction} = 773$ K; H_2O/ethanol = 0.0 (for ED); H_2O/ethanol = 2.0 (for SR and OSR); O_2/ethanol = 0.5 (for POX and OSR) and residence time = 0.02 g s/mL).

For each reaction tested, the decrease in hydrogen selectivity was accompanied by an increase in acetaldehyde selectivity; in fact, acetaldehyde was the main product observed during ED. Significant amounts of ethene were detected only during ED, and its selectivity remained virtually constant during 6 h TOS.

The selectivity of CO_2 increased slightly during the ED, SR, POX, and OSR reactions. Moreover, CO production was detected only for the SR and POX reactions and was much more significant in the reaction that contained oxygen in the feed. For SR, CO selectivity decreased significantly at the beginning of the reaction test; in fact, CO was no longer detected after 1 h TOS. In contrast, CO formation remained relatively constant during POX. Methane selectivity was low and constant for ED, SR, and POX; higher methane formation was observed for OSR.

Table 1 displays the product distribution results obtained on a dry basis at the same level of conversion (~60%, 773 K) for all of the reactions studied. Hydrogen was observed only during ED and SR, and its selectivity was higher during SR, in which the selectivity to acetaldehyde was lower. CO_2 selectivity was higher in both OSR and POX, whereas CO selectivity was greater in POX. These results indicate that adding water to the feed increased the production of H_2, CO, and CO_2 and decreased the selectivity to acetaldehyde; moreover, no significant amount of ethene was detected in the product. The increases in H_2, CO, and CO_2 selectivity likely can be ascribed to the reaction between water and ethanol.

Table 1
Product distributions obtained on a dry basis at the same conversion (~60%) for ED, SR, POX and OSR for $Pt/CeZrO_2$ catalyst[a]

Reaction	Product distribution (%)					
	H_2	CH_4	CO	CO_2	Acetaldehyde	Ethene
ED	45	3	2	2	36	12
SR	65	7	9	14	5	0
POX	0	4	16	39	40	1
OSR	0	15	0	40	44	1

[a] $T_{reaction} = 773$ K; H_2O/ethanol = 2.0 (for SR and OSR); O_2/ethanol = 0.5 (for POX and OSR) and residence time = 0.02 g s/mL.

Similar results were obtained by Kugai et al. [28] for ED, SR, POX, and OSR over a $Ni–Rh/CeO_2$ catalyst. These authors found the highest H_2 production rates for ED and SR. They also reported that POX and OSR exhibited the highest CO_2 selectivity, whereas CO production was greatest during POX. It should be pointed out that the product distributions presented by these authors for the different reactions were not obtained at the same conversion level. Ethene is produced by the dehydration of ethanol ($C_2H_5OH \rightarrow C_2H_4 + H_2O$) [4], which is not favored in the presence of water.

The product distributions also indicate that the addition of O_2 did not have a positive effect on H_2 selectivity, likely due to oxidation to water. On the other hand, the presence of O_2 favored the production of CO_2 and acetaldehyde.

SR, POX, and OSR also were carried out without catalyst (homogeneous reactions) at 773 K (not shown). The results differed significantly from those obtained for the $Pt/CeZrO_2$ catalyst. In the absence of this catalyst, the ethanol conversion was lower for all reactions (~25% for SR and POX and ~60% for OSR). For SR and POX, the main product was acetaldehyde, whereas for OSR, large amounts of acetaldehyde, methane, and CO_2 were observed. SR was studied in greater detail, because the highest stable H_2 production and the lowest byproduct formation were obtained for this reaction.

3.2.1. Effect of H_2O/ethanol molar ratio during SR over $Pt/CeZrO_2$

The foregoing results indicate that the highest H_2 production rates after 6 h TOS were obtained for SR, but the catalysts underwent significant deactivation. To explore the impact of H_2O on the stability of the $Pt/CeZrO_2$ catalyst, the effect of the H_2O/ethanol molar ratio during SR at 773 K was evaluated.

Fig. 2 presents ethanol conversion and product distributions as functions of TOS obtained for the $Pt/CeZrO_2$ catalyst during SR with H_2O/ethanol molar ratios of 3.0 and 5.0. Comparing the results in Figs. 1b, 2a, and 2b shows that increasing the H_2O/ethanol molar ratio from 2.0 to 3.0 increased the initial ethanol conversion, but that increasing the H_2O/ethanol molar ratio further from 3.0 to 5.0 produced no additional benefit. This finding strongly suggests that adding more water to the feed favored the SR pathway. Despite the increase in initial conversion, increasing the H_2O/ethanol molar ratio did not promote long-term catalyst stability. Although a short-term improvement in the catalyst deactivation rate was observed initially with higher H_2O/ethanol molar ratios, a high rate of deactivation was found at all H_2O/ethanol molar ratios studied. Nevertheless, for H_2O/ethanol molar ratios of 2.0 (Fig. 1b) and 3.0 (Fig. 2a), the catalyst became stable after an initial deactivation period, but deactivated continuously (albeit more slowly initially) at a H_2O/ethanol molar ratio of 5.0 (Fig. 2b). A strong deactivation of the Rh/CeO_2–ZrO_2 catalyst also was observed for SR even at a high steam-to-ethanol molar ratio (H_2O/ethanol = 8.0) [29].

Vaidya and Rodrigues [3] reviewed the kinetic studies of the SR of ethanol and found that many authors have reported a first order for the reaction with respect to ethanol. In our work, the initial rate of reaction and the turnover frequency (TOF) were calculated considering a first-order reaction and the Pt dispersion determined by CH dehydrogenation. For a first-order reaction, the rate constant k at 773 K was 7.6×10^5 $cm^3/(g_{cat}\,h)$, and the activation energy obtained was 50.3 kJ/gmol. In the literature, the values of activation energy vary significantly, from 1.87 to 149 kJ/gmol. The initial rate and TOF calculated at 773 K were 0.6 gmol/(g_{cat} h) and 9.8 s^{-1}, respectively.

H_2 production decreased at the beginning of the reaction test for H_2O/ethanol molar ratios of 2.0 and 3.0, but then remained relatively stable thereafter. With a H_2O/ethanol molar ratio of 5.0, the selectivity to H_2 remained quite stable for the first 4 h TOS, followed by a decrease thereafter. This decrease in H_2 selectivity was accompanied by an increase in acetaldehyde selectivity. Small quantities of CH_4, CO, and CO_2 and trace amounts of ethene were seen at all H_2O/ethanol molar ratios evaluated. Dömök et al. [18] also detected a decrease in H_2 selectivity and an increase in acetaldehyde selectivity during SR over an alumina-supported Pt catalyst, using H_2O/ethanol molar ratios of 3.0 and 9.0.

Table 2 presents the product distributions obtained on a dry basis at the same level of conversion (~55%) for different H_2O/ethanol molar ratios. Increasing this ratio resulted in a beneficial effect on the H_2 and CO_2 production rates. Furthermore,

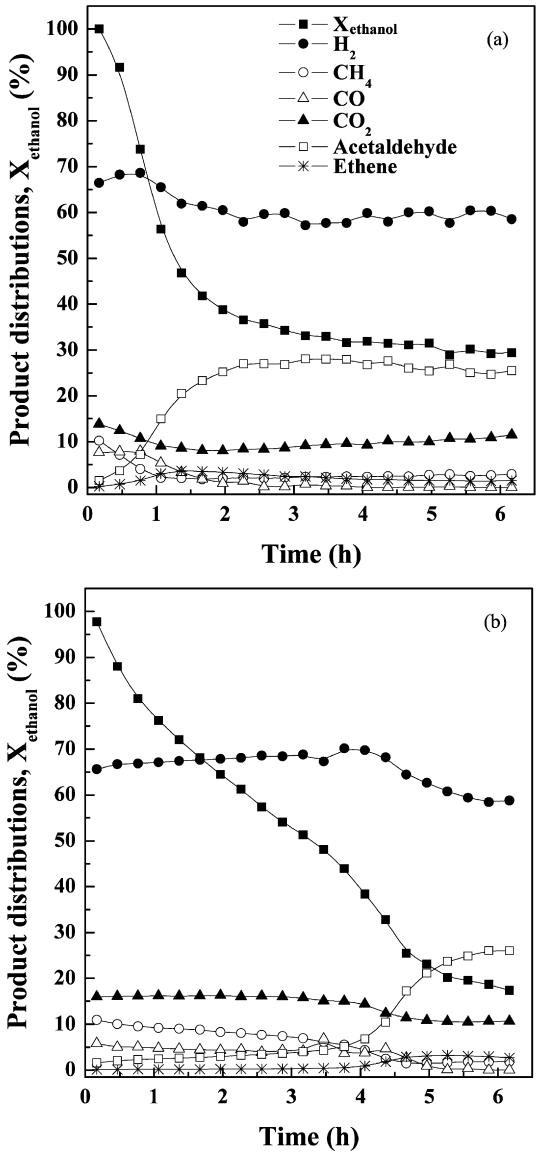

Fig. 2. Ethanol conversion ($X_{ethanol}$) and product distributions versus time on stream obtained during on SR at (a) H_2O/ethanol molar ratio = 3.0 and (b) H_2O/ethanol molar ratio = 5.0 for $Pt/CeZrO_2$ catalyst ($T_{reaction}$ = 773 K and residence time = 0.02 g s/mL).

Table 2
Product distributions obtained on a dry basis at the same level of conversion (~55%) during SR at H_2O/ethanol molar ratios of 2.0, 3.0 and 5.0 over $Pt/CeZrO_2$ catalyst[a]

H_2O/ethanol molar ratio	Product distribution (%)					
	H_2	CH_4	CO	CO_2	Acetaldehyde	Ethene
2.0	63	4	10	11	10	2
3.0	66	2	5	9	15	3
5.0	69	8	4	16	3	0

[a] $T_{reaction}$ = 773 K and residence time = 0.02 g s/mL.

increasing the H_2O/ethanol molar ratio from 2.0 to 5.0 resulted in a decrease in CO production. These results are in agreement with those reported by several authors [31–34] for SR over Ni-based catalysts. According to these authors, adding water favored the water–gas shift reaction, leading to an increase in H_2 and CO_2 production along with a decrease in CO formation.

Increasing the H_2O/ethanol molar ratio from 3.0 to 5.0 was found to lead to a decrease in acetaldehyde and ethene formation. These results are consistent with the findings of Dömök et

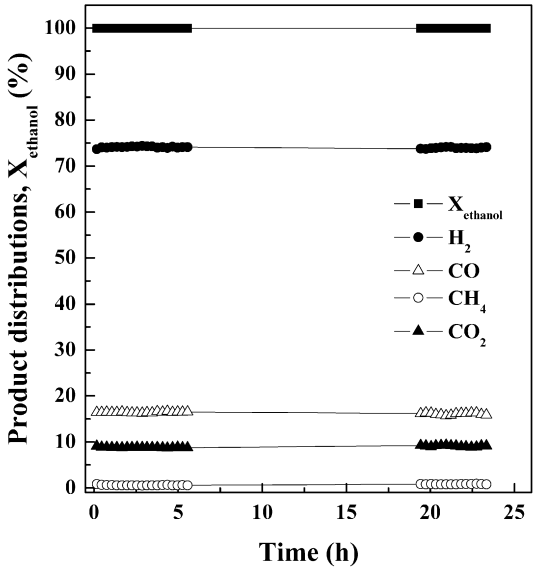

Fig. 3. Ethanol conversion ($X_{ethanol}$) and product distributions versus time on stream obtained during SR over Pt/$CeZrO_2$ catalyst at 1073 K (H_2O/ethanol molar ratio = 3.0 and residence time = 0.02 g s/mL).

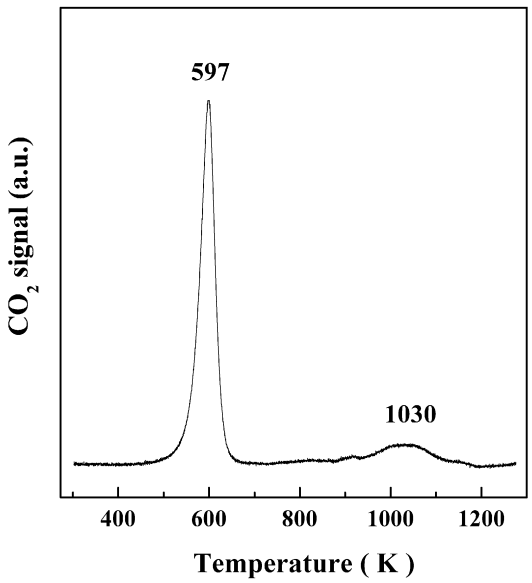

Fig. 4. TPO profile of Pt/$CeZrO_2$ catalyst obtained after SR at 773 K (H_2O/ethanol molar ratio of 3.0 and residence time = 0.02 g s/mL).

al. [18], who reported that increasing the H_2O/ethanol molar ratio from 3.0 to 9.0 led to a decrease in ethene production during SR over alumina-supported Pt catalysts. As described earlier, water inhibits the dehydration of ethanol, thereby limiting the amount of ethene produced. It is noteworthy that acetaldehyde selectivity increases with catalyst deactivation. In fact, accompanying the initial improvement in deactivation rate with increasing H_2O/ethanol ratio, the onset time of the rise in acetaldehyde selectivity increases significantly. Further discussion of the effect of H_2O/ethanol molar ratio on deactivation rate and product selectivity changes is presented in terms of the proposed mechanism following the DRIFTS analysis.

3.2.2. *Effect of the reaction temperature on SR over Pt/$CeZrO_2$*

According to the literature, SR proceeds through different pathways, depending on the reaction temperature. At low reaction temperatures, byproducts formed include oxygenated compounds (e.g., acetaldehyde, acetone) and hydrocarbons (e.g., methane, ethane). Ethene is considered a precursor to coke formation, which in turn contributes to catalyst deactivation. On the other hand, high-temperature SR favors the thermodynamic equilibrium composition, including the production of CO at levels >10 ppm, which will poison the electrodes of PEM fuel cells if not converted. Therefore, additional CO conversion and cleanup steps are required in the fuel processor. Interestingly, metal-doped, ceria-containing catalysts also exhibit good activity for the water–gas shift and preferential oxidation reactions [35], features that may allow the future design of an integrated processor based on one main catalyst system.

In the present work, SR was carried out at two temperatures: 773 K (low reaction temperature) and 1073 K (high reaction temperature). Figs. 2a and 3 present ethanol conversion ($X_{ethanol}$) and product distributions during SR over the Pt/$CeZrO_2$ catalyst at 773 K and 1073 K, respectively. The catalyst exhibited the same initial ethanol conversion level at both temperatures; however, increasing the reaction temperature from 773 to 1073 K greatly improved the catalyst stability, such that it remained quite stable at the higher temperature. Some authors [31,34,36] have reported that a decrease in reaction temperature leads to carbon accumulation on the surface of supported metal catalysts, resulting in loss of catalytic activity during SR. When the reaction temperature is increased, the carbon deposition rate decreases. This phenomenon has been attributed to both thermodynamic and kinetic factors [34]. Whereas lower temperatures (<823 K) thermodynamically favor the production of coke, from a kinetic standpoint, higher temperatures facilitate carbon removal (e.g., the reactions of carbon with steam or CO_2) [34]. In addition, Roh et al. [29] linked the rapid deactivation of a Rh/CeO_2–ZrO_2 catalyst during SR to carbon deposition on the catalyst surface. According to these authors, catalyst deactivation was closely correlated with ethene formation, which is considered a carbon precursor.

Concerning product distributions, H_2, CO, CO_2, acetaldehyde, and ethene were observed at low temperatures, whereas H_2, CO, and CO_2 were the only products detected at high temperatures. Several authors [31–34,36,37] have reported that increasing the reaction temperature decreases acetaldehyde and ethene formation in favor of H_2, CO, and CO_2 production during SR over Ni- and Rh-based catalysts. These results have been attributed to acetaldehyde and ethene reforming reactions at high temperatures, which increase the production of H_2, CO, and CO_2.

Comparing the product distributions obtained with the thermodynamic equilibrium composition [38–40] clearly shows that the product composition is far from thermodynamic equilibrium at 773 K but is closer to thermodynamic equilibrium at 1073 K. These results agree with those reported by Roh et al. [6] for SR over Rh/Al_2O_3 and Rh/CeO_2–ZrO_2 catalysts, who found a H_2 yield close to the equilibrium value for both catalysts only at temperatures above 773 K.

Because the activity of Pt/$CeZrO_2$ decreased significantly during the reaction at low temperature (773 K), TPO experiments were carried out after 6 h TOS to study the nature of the carbonaceous species formed that can contribute to catalyst deactivation. The TPO profile, shown in Fig. 4, exhibited two peaks around 597 and 1030 K, corresponding to CO_2 formation, with the low-temperature peak much more prominent than the high-temperature peak. Roh et al. [29] detected a CO_2 peak at around 480 K for Rh/CeO_2–ZrO_2 catalysts during TPO experiments performed after SR at 623 K; the CO_2 evolved was assigned to the oxidation of carbonaceous deposits. Erdohelyi et al. [17] reported that hydrogen selectivity decreased while acetaldehyde formation increased during the reaction, in agreement with our findings in the present work. According to these authors, the decrease of hydrogen selectivity during SR was due to an inhibiting effect of surface acetate species. They pro-

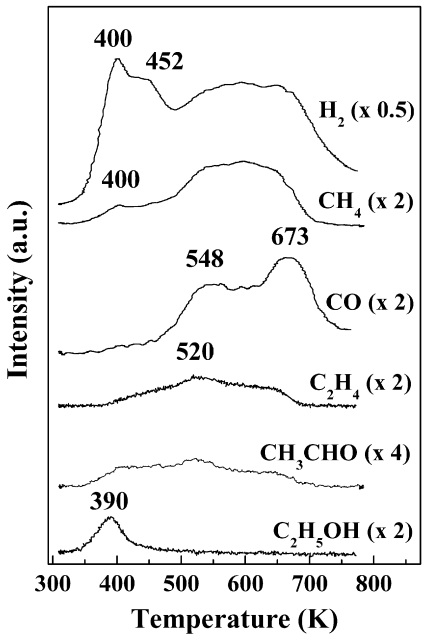

Fig. 5. TPD profile of $Pt/CeZrO_2$ catalyst obtained after ethanol adsorption at room temperature.

posed that the highly stable acetate species adsorbed on the support hindered the migration of the ethoxy species from the support to the metal particles and, consequently, its decomposition. Recently, Platon et al. [41] studied the deactivation of $Rh/Ce_{0.8}Zr_{0.2}O_2$ catalysts in low-temperature SR. Transmission electron microscopy (TEM) analysis detected no significant metal particle sintering or carbon deposition, whereas thermogravimetric analysis (TGA) and TPO analysis revealed a significant buildup of carbonaceous intermediates, causing catalyst deactivation. These carbonaceous intermediates were less stable at higher reaction temperatures. Among the reaction intermediates, acetone and ethene were mainly responsible for the catalyst deactivation.

In the present work, the peaks at 597 and 1030 K likely can be attributed to the oxidation of two different carbonaceous deposits: carbon-containing surface species and carbon deposits over the $CeZrO_2$ support, respectively. This suggests that the deactivation of $Pt/CeZrO_2$ catalyst at 773 K likely was related to the presence of acetate-like surface species, as discussed in more detail in the next section. On the other hand, at high temperatures (>823 K), the formation of coke during SR is not thermodynamically favored [34] or the acetate species are not stable, likely contributing to the stability of $Pt/CeZrO_2$ at 1073 K.

3.3. Reaction mechanism

3.3.1. TPD of ethanol

Fig. 5 presents the TPD profiles of adsorbed ethanol for the $Pt/CeZrO_2$ catalyst. Ethanol desorption was detected only at 390 K. Similar results have been reported previously for the TPD of ethanol over supported metal catalysts [13,17]. In addition, small amounts of acetaldehyde and ethene were detected between 351 and 703 K, reaching a maximum at around 520 K. Erdohelyi et al. [17] also reported the production of acetaldehyde and ethene at around 500 K over CeO_2- and Al_2O_3-supported noble metal catalysts and suggested that this was due to the dehydrogenation and dehydration of ethanol, respectively.

At low temperatures, the $Pt/CeZrO_2$ catalyst exhibited a significant peak for H_2 production (at 400 and 450 K) and a smaller peak for CH_4 formation (at 400 K). The formation of H_2, CH_4, and CO in the low-temperature region during the TPD of ethanol over Al_2O_3- and CeO_2-supported metals has been reported previously [13,14,42–44]; those studies suggested that ethanol adsorbs on the catalyst surface as ethoxy species that can be decomposed to H_2, CH_4, and CO on metal particles. The absence of CO desorption in the present study suggests that CO remained adsorbed at low temperatures.

At high temperatures, two broad peaks (at 490–730 K) related to both H_2 and CH_4 formation were detected for the $Pt/CeZrO_2$ catalyst, whereas CO desorption was observed at 548 and 673 K. No significant production of CO_2, crotonaldehyde, acetone, or benzene was detected by TPD analysis. Several previous studies [13,42,43] detected the formation of CO and CH_4 at high temperatures (above 500 K) during TPD of ethanol over CeO_2 and Al_2O_3 supports, and assigned their formation to the products of decomposition of carbon species (i.e., acetaldehyde and acetate species) formed previously. According to these studies, a fraction of acetate species can be oxidized to carbonate species that are decomposed to CO_2. It also was reported that a greater amount of CO_2 was desorbed from alumina than over ceria support [13]. According to the literature [45], CO_2 can replenish the oxygen vacancies of the CeO_2 support, releasing CO as a product. Because alumina does not have a significant population of oxygen vacancies, the CO_2 formation rate is likely higher on this support. In the present work, the OSC analysis demonstrated a high density of oxygen vacancies in the $Pt/CeZrO_2$ catalyst, which can explain the absence of CO_2 and the large desorption peak assigned to CO at high temperatures during the TPD experiments. Finally, the high H_2 production detected at high temperature in the TPD profiles of the $Pt/CeZrO_2$ catalyst can be assigned to the desorption of H_2 previously formed during the steps of ethanol dehydrogenation.

Comparing the TPD results obtained for $Pt/CeZrO_2$ catalyst with those reported in the literature for the Pt/CeO_2 catalyst [13] shows greater formation of CH_4 and CO at high temperatures for the $CeZrO_2$-supported catalyst. This finding suggests that adding Zr to ceria promoted the decomposition of carbon species formed previously (acetaldehyde and acetate species). In addition, CO_2 formation was detected only for the Pt/CeO_2 catalyst. As reported previously [24], the $Pt/CeZrO_2$ catalyst had a much greater OSC than the Pt/CeO_2 catalyst; therefore, the dissociation of CO_2 on oxygen vacancies of the support was favored on $Pt/CeZrO_2$, which is consistent with the higher formation of CO during TPD of ethanol on the $CeZrO_2$-supported catalyst.

3.3.2. DRIFTS

3.3.2.1. DRIFTS analysis of ethanol desorption Fig. 6 shows the IR spectra of adsorbed ethanol on the $Pt/CeZrO_2$ catalyst at different temperatures. At room temperature, the bands at 1045, 1081, 1407, 1452, 1473, 2880, 2906, 2935, and 2977 cm^{-1} correspond to different vibrational modes of ethoxy species, which were formed by dissociative adsorption of ethanol [13,14,46–48]. According to the literature [46], the ethoxy species adsorb over Ce cations in bidentate and monodentate modes. The ethoxy bands are shifted to lower wavenumbers when ethoxy species are adsorbed on a Ce cation close to an oxygen vacancy. In our work, the low wavenumber band positions ascribed to ν(CO) of adsorbed ethoxy suggest that the adsorbed ethoxy species are type II, analogous to the type II methoxy species observed over partially reduced ceria [49,50]; that is, the ethoxy species are associated with Ce^{3+} atoms on the surface of ceria, consistent with surface shell reduction [20]. Actually, TPR profiles of $Pt/CeZrO_2$ catalyst revealed that ceria surface shell is completely reduced below 700 K, confirming that ethoxy species are adsorbed over Ce^{3+} cations. Furthermore, the formation of ethoxy species from adsorption of ethanol over Ce^{3+} cations (i.e., oxygen vacancy defects) occurs simultaneously with the formation of hydroxyl groups by dissociation of the ethanol molecule. During ethanol adsorption, a decrease in a band

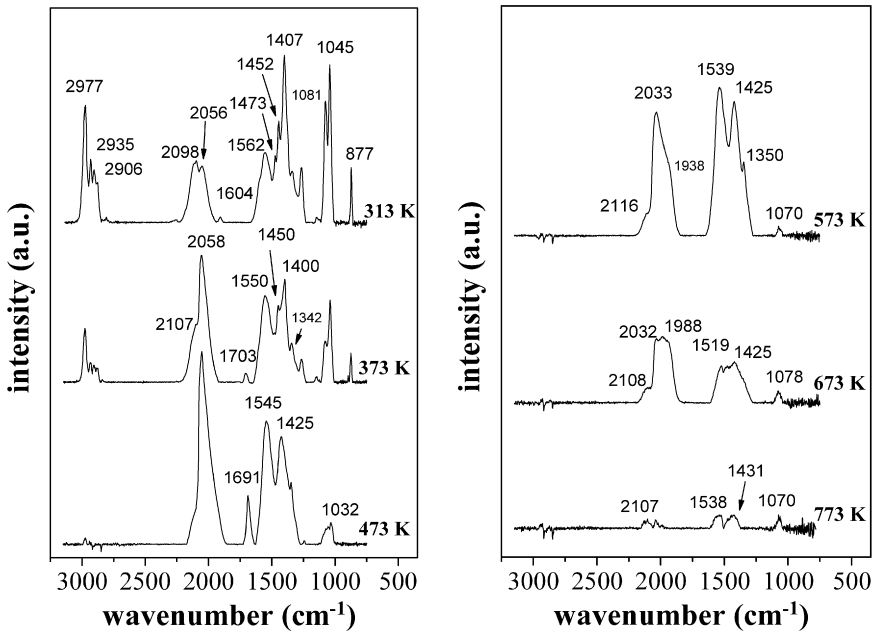

Fig. 6. DRIFTS spectra of adsorbed ethanol on $Pt/CeZrO_2$ catalyst at different temperatures.

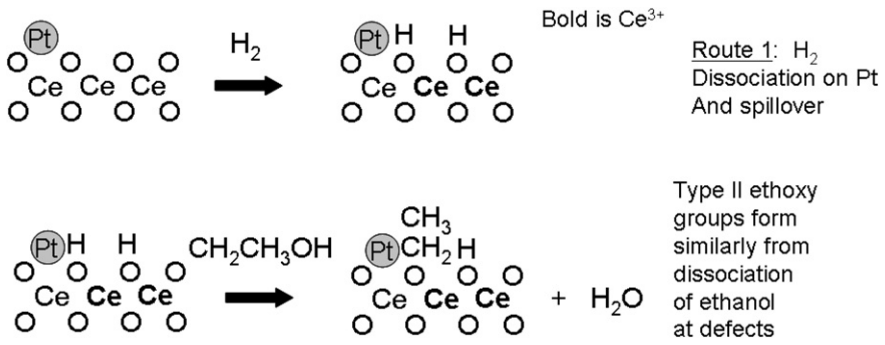

Scheme 1. Activation of ethanol by type II ethoxy group formation.

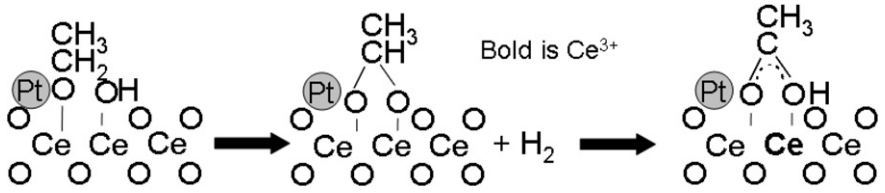

Scheme 2. Transformation of ethoxy to acetate species by surface O.

at ~3650 cm^{-1} indicates that ethanol adsorption displaces H_2O that was dissociated at O vacancies, according to Scheme 1.

In addition to the bands of ethoxy species, there are also bands at 1342 and 1562 cm^{-1}, which are assigned to the ν(OCO) symmetric and asymmetric vibrational modes of acetate species that develop on the catalyst surface [13,14,46–48]. The appearance of these bands indicates that ethoxy species were somehow oxidized to acetate species. One widely held view is that the transformation from ethoxy species to acetate species over ceria-containing catalysts is attributed to the redox properties of the support [13]. This reaction involves the dehydrogenation of ethoxy species to acetaldehyde, which may be further dehydrogenated to acetyl species. This intermediate may react with oxygen from the support to produce the acetate species [51], as shown in Scheme 2.

Other possible routes to acetate formation also should be considered. Erdohelyi et al. [17] suggested that acetate species are formed via two reaction pathways: (i) the reaction between the acetyl species and the oxygen from the support and/or (ii) acetaldehyde reaction with the surface OH groups. A route from ethoxy to acetate involving OH groups (i.e., promoted by adsorbed H_2O) at moderate temperatures over Pt/ceria during SR containing a H_2 cofeed also has been postulated [20].

In our work, however, the surface was completely reduced by the H_2 treatment and then covered by type II bridging OH groups [49]. Therefore, because the density of O^* atoms available for reaction should be low in this case, a route from ethoxy to acetate involving type II bridging OH groups appears more likely; such a mechanism was postulated over Pt/ceria after ethoxy species were observed to completely convert to acetate species in DRIFTS after steaming at 433 K [20], as described in Scheme 3. Thus, Scheme 2 may be favored when O_2 is included in the feed, whereas Scheme 3 may be favored when H_2O or another source

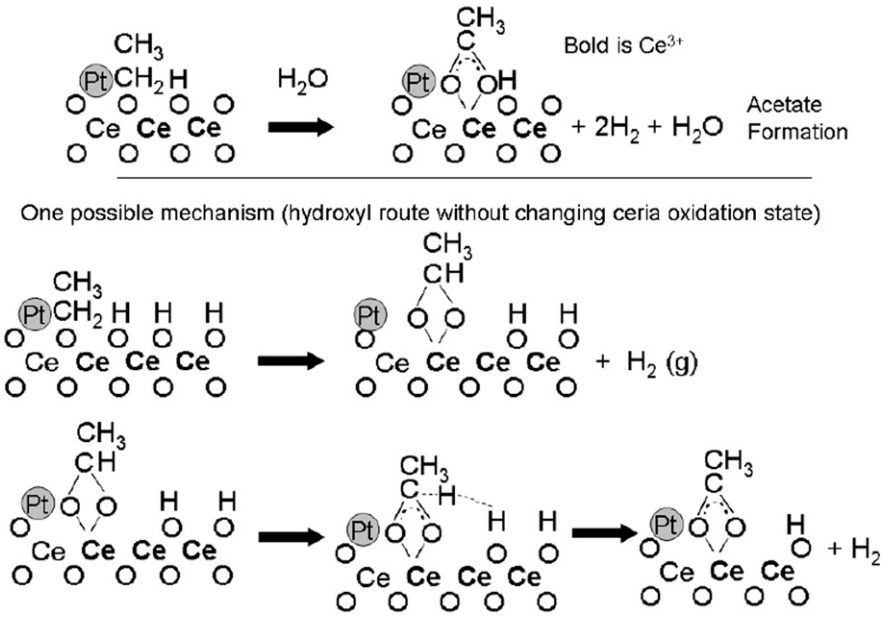

Scheme 3. Transformation of ethoxy to acetate species by surface OH.

of –OH is present, unless it is proven that H_2O reoxidizes the ceria.

The bands at 2056 and 2098 cm^{-1} have been attributed to the ν(CO) vibrational modes of linearly adsorbed CO on metal particles [52–54]. The band at 2056 cm^{-1} has been assigned to the ν(CO) mode of CO adsorbed on small Pt particles, whereas the band at 2098 cm^{-1} corresponds to the ν(CO) mode of linear CO bound to large Pt particles. TPD of adsorbed ethanol (Fig. 5) revealed the formation of methane and hydrogen between 300 and 480 K. This result has been attributed to the ED reaction [13,14,17,18,46,47]. The CO produced remained adsorbed on the Pt surface. Dömök et al. [18] monitored the gas-phase composition during IR experiments by mass spectrometry and observed the formation of hydrogen and methane, confirming that ED occurred. According to these authors, the decomposition of both ethoxy and acetaldehyde species contribute to the formation of methane, hydrogen, and CO.

When the catalyst was heated to 373 K, the intensity of the bands corresponding to ethoxy species strongly decreased, whereas the intensity of the bands assigned to CO adsorbed on metal particles increased. This result confirms that ethanol decomposes into CO, methane, and hydrogen. The spectrum also exhibited a weak band around 1703 cm^{-1}, which was attributed to the ν(CO) mode of adsorbed acetaldehyde [16,18,55].

At 473 K, the bands associated with ethoxy species completely disappeared, whereas the bands assigned to acetate species (1545 and 1425 cm^{-1}) remained unchanged. The intensity of the bands corresponding to acetaldehyde (1691 cm^{-1}) and CO (2058 cm^{-1}) increased strongly.

Increasing the temperature to 573 K led to an increase in the intensity of the bands related to acetate species, while the intensity of the CO bands decreased and the acetaldehyde band disappeared. At temperatures above 573 K, the intensities of the bands of acetate species and adsorbed CO strongly decreased, and at 773 K, bands were no longer detected. Comparing the results with the TPD data clearly shows two CO and CH_4 peaks at 500–750 K, consistent with the acetaldehyde and acetate decomposition observed in DRIFTS. During TPD and DRIFTS experiments, the amount of H_2O present may be low, in which case, H_2O may not assist in CO_2 desorption from the surface by dissociation at the vacancies. One result may be that CO_2 reoxidizes the vacancy, liberating CO in the process, which is consistent with the TPD data and similar to a mechanism proposed during CO_2 reforming in the CH_4 reaction [45]. This may explain the absence of CO_2 in both experiments. Both H_2O-assisted and -unassisted acetaldehyde and acetate demethanation reactions are described in Scheme 4.

It is useful to consider that the foregoing H_2O-assisted acetate decomposition reaction to methane and carbonate is the analog of forward formate decomposition [56], where in the presence of H_2O, both the formate turnover rate (as low as ~403 K required) and the decomposition selectivity are promoted, such that H_2 and CO_2 (product of carbonate decomposition) are produced.

Another possible route for CO formation may be explained by examining the analog of formate decomposition. In that case, thermal formate decomposition [56] favors the reverse pathway, back to CO and –OH*, and requires higher temperature (~573 K). The analog of reverse acetate decomposition would be CO and $–OCH_3^*$. In the presence of –OH*, the methoxy group would undergo transformation to formate, which can subsequently decompose either in the forward direction (i.e., to H_2 and CO_2) or the reverse direction (i.e., to –OH and CO), depending on whether or not coadsorbed H_2O is present. The forward/reverse decomposition reactions of formate, along with the proposed acetate analog, are provided in Scheme 5.

3.3.2.2. DRIFTS analysis of ED Fig. 7 shows the DRIFTS spectra at different temperatures and under ethanol flow. At room temperature, the spectrum is approximately identical to that shown in Fig. 6, as expected. The bands corresponding to ethoxy species (at 1045, 1081, 1408, 1452, 2811, 2898, 2935, and 2978 cm^{-1}), acetate species (at 1336 and 1562 cm^{-1}), and CO adsorbed linearly (at 2048 and 2098 cm^{-1}) are observed.

Increasing the temperature to 373 K strongly increased the intensity of the bands assigned to acetate species. In the case of the DRIFTS analysis of adsorbed ethanol (Fig. 6), the intensity of the acetate bands remained practically unchanged, indicating that the oxidation of ethoxy species to acetate species is more significant as ethanol flows continuously through the catalyst. The intensity of the band related to CO linearly adsorbed increased slightly, while the bands assigned to ethoxy species decreased.

In contrast, the spectrum exhibited significant differences when the catalyst was heated to 473 K under ethanol flow. The intensity of the bands corresponding to linearly adsorbed CO increased,

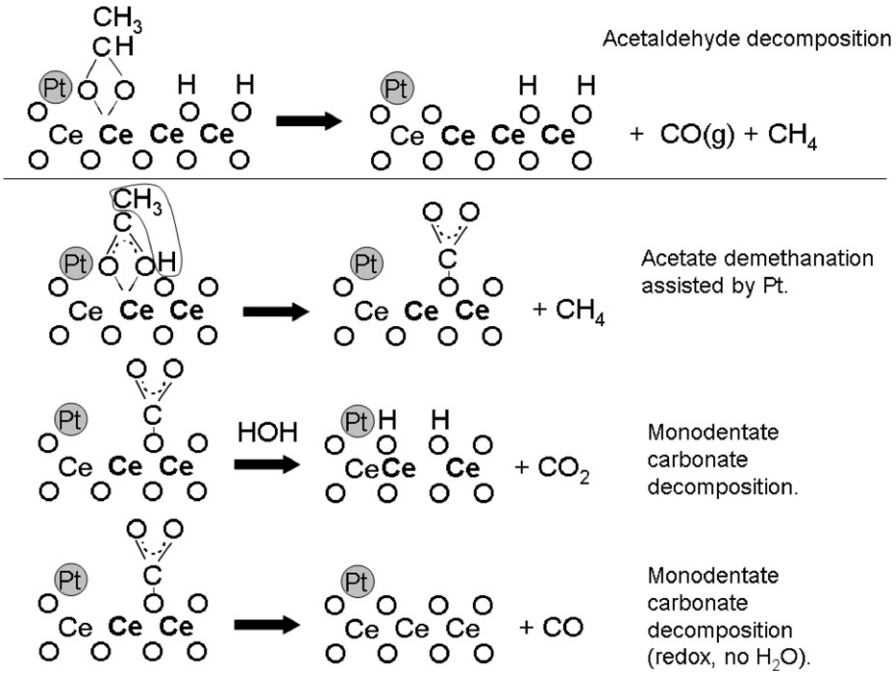

Scheme 4. Acetaldehyde decomposition and acetate demethanation.

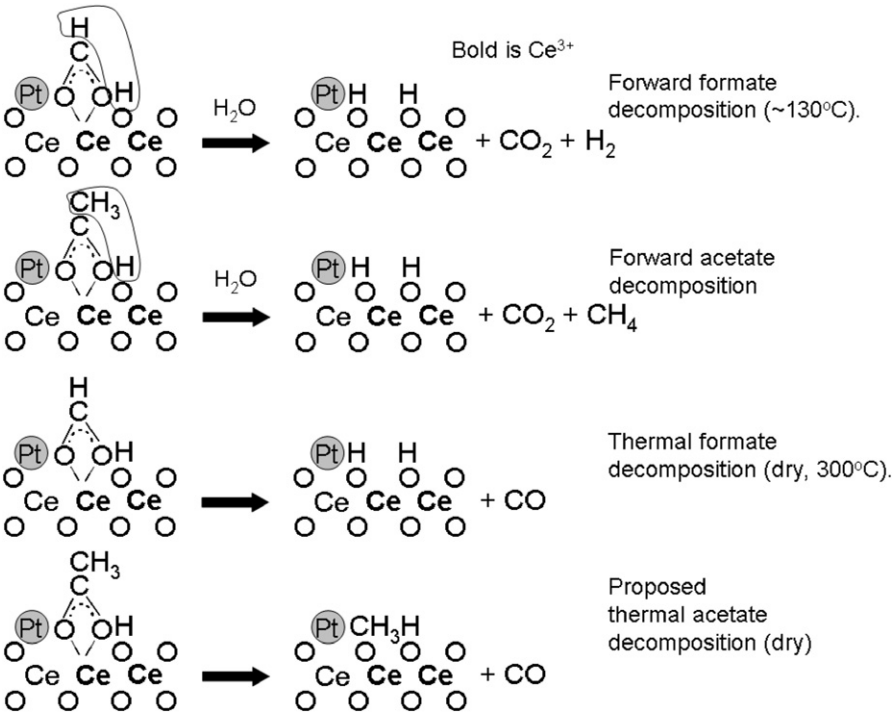

Scheme 5. Forward versus thermal decomposition of formate, acetate.

whereas that of the bands attributed to acetate species strongly increased. Furthermore, the appearance of the bands at 2330 and 2360 cm^{-1} indicates that CO_2 was formed at this temperature. Comparing these results with those obtained during DRIFTS analysis of adsorbed ethanol at 473 K (Fig. 6) suggests that the surface concentration of acetate species formed was higher and that CO_2 formation could be detected only when ethanol was flowing through the catalyst.

Actually, ethanol adsorption and dissociation to ethoxy species occurred continuously as ethanol flowed through the catalyst. The oxidation reaction of ethoxy species to acetate occurred instantaneously on the catalyst surface, because the bands of ethoxy species were hardly detected, as shown in Fig. 7. It has been reported that acetate species formed previously can be decomposed to CO_2 via carbonate species [14,20,46,47]. As discussed previously, Jacobs et al. [20] postulated that the presence of type II OH groups associated with Ce^{3+} defect sites aids in the transformation from acetate to methane and carbonate, the latter of which decomposes further to CO_2, as described in Scheme 4.

At 573 K, the intensity of the bands assigned to CO and CO_2 increased, whereas the acetate bands decreased slightly. Further heating to 673 K decreased the intensity of the acetate species

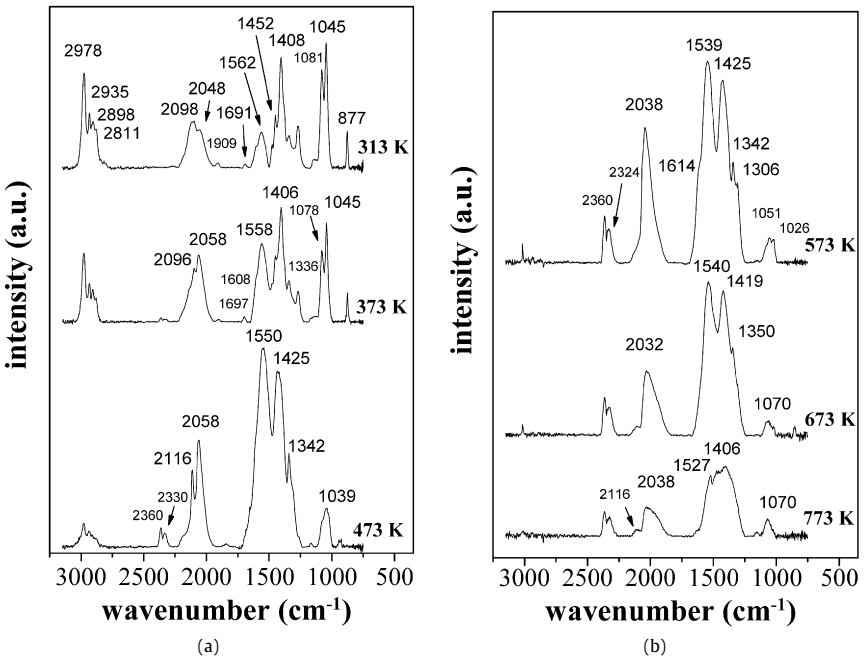

Fig. 7. DRIFTS spectra obtained on $Pt/CeZrO_2$ catalyst at different temperatures and ethanol flow.

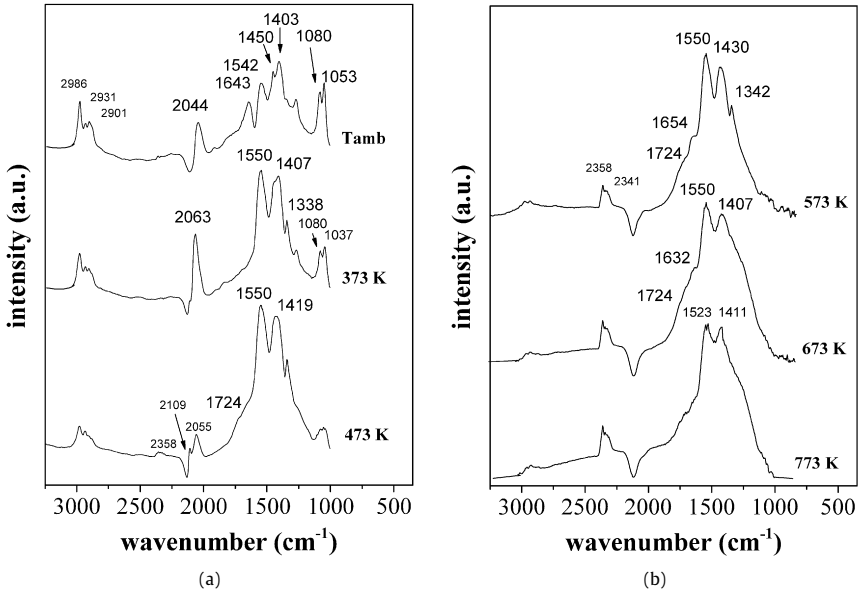

Fig. 8. DRIFTS spectra obtained on $Pt/CeZrO_2$ catalyst at different temperatures and under the reaction mixture containing ethanol and oxygen (ethanol/oxygen ratio = 0.5).

as well as the adsorbed CO band; however, both bands practically disappeared at high temperatures during DRIFTS analysis of the TPD of adsorbed ethanol (Fig. 6). At high temperatures (i.e., 773 K), there remained bands attributed to CO, CO_2, and acetate species, whereas no bands were detected in the previous DRIFTS spectrum for the TPD of adsorbed ethanol at high temperatures.

The formation of acetate species merits additional comments. As described in Schemes 2 and 3, acetate species may be formed either by the reaction of acetyl species with oxygen from the support or via hydroxyl groups. The presence of acetate species even at 773 K indicates that the reaction with hydroxyl groups is the most likely reaction route. The support will not likely have available oxygen to supply after the analysis of the same sample at different temperatures, unless the ethanol feed itself can replenish the vacancies of the support with O*. The hydroxyl groups are formed during different dehydrogenation steps of ethanol, as described in Scheme 2.

3.3.2.3. DRIFTS analysis under an ethanol–oxygen mixture Fig. 8 shows the DRIFTS spectra obtained for the reaction mixture containing ethanol and oxygen (ethanol/oxygen ratio = 0.5). Basically, the spectrum at room temperature exhibited the same bands observed during the DRIFTS analysis after ethanol adsorption (Figs. 6 and 7): ethoxy species (1053, 1080, 1403, and 1450 cm^{-1}), acetate species (1542 cm^{-1}), and linearly adsorbed CO (2044 cm^{-1}). In this case, a new band was detected at around 1643 cm^{-1}, attributed to the ν(CO) vibrational mode of acetyl species [16,55]. This intermediate stems from hydrogen elimination of the adsorbed acetaldehyde. The main difference between the spectra at room temperature in Figs. 6 and 8 is that the acetate/ethoxy ratio was higher when O_2 was co-fed. This result can be explained in

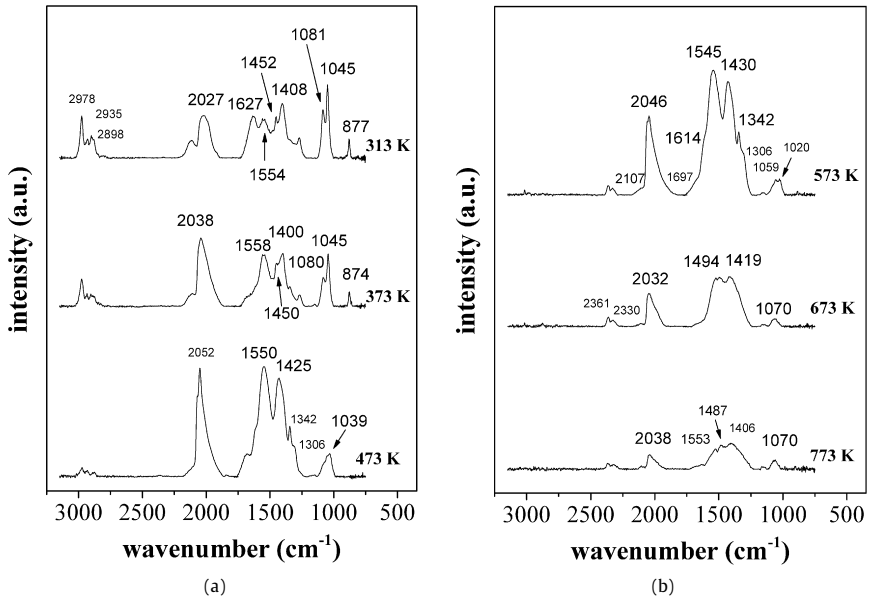

Fig. 9. DRIFTS spectra obtained on $Pt/CeZrO_2$ catalyst at different temperatures and under the reaction mixture containing ethanol and water (water/ethanol ratio = 2.0).

terms of the redox properties of the support. Oxygen of the feed partially replenishes the vacancies of the support, making more oxygen available to oxidize the ethoxy species to acetate species, as described in Scheme 2. In addition, the intensity of the ν(CO) band characteristic of CO linearly adsorbed on Pt is lower in the presence of oxygen, likely as a direct consequence of the higher fraction of ethoxy species converted to acetate species under the reaction conditions.

Increasing the temperature to 373 K strongly increased the intensity of the band associated with acetate species and also decreased the intensity of the bands of ethoxy and acetyl species.

At 473 K, the intensity of the bands of acetate species still increased. In addition, the branches of the band corresponding to CO_2 formation (2357 and 2341 cm^{-1}) became visible. This result is very similar to that observed during DRIFTS under ethanol flow, but with the appearance of the band at 1724 cm^{-1}, which is attributed to acetaldehyde [16,18,55]. It is important to note that the formation of acetaldehyde was significantly higher under the ethanol/O_2 reaction mixture.

Increasing the temperature to 573 K led to the disappearance of bands characteristic of the ethoxy species and linearly adsorbed CO. In this case, the spectrum exhibited only bands corresponding to acetate species, acetaldehyde, and CO_2.

Heating the catalyst to 673 K did not result in significant changes to the spectrum; only the intensity of the acetate species bands decreased slightly. At 773 K, the bands attributed to acetate species were no longer detected, whereas the bands characteristic of carbonate species (1523 and 1411 cm^{-1}) were now present.

Comparing the DRIFT spectra in the high-temperature range (573–773 K) revealed marked differences between the set of spectra recorded using ethanol alone and that recorded during the co-feeding of ethanol and oxygen. The presence of the CO band in the spectrum under ethanol flow suggests that adding oxygen to the feed inhibited the reaction of ethanol decomposition or promoted the oxidation of CO to CO_2. Acetaldehyde was detected mainly under an ethanol/oxygen mixture. Oxidative ethanol dehydrogenation is a commercial technology for acetaldehyde production. The bands corresponding to carbonate species were more intense when the ethanol–oxygen mixture was used. In this case, the oxidation of ethoxy species to acetate, followed by decomposition to CO_2 via carbonates species, may use oxygen from the support, because the vacancies are continuously replenished by oxygen from the feed; however, the participation by hydroxyl groups cannot be ruled out entirely. Actually, both reaction pathways may explain the greater formation of acetate and carbonate species during the experiment with co-fed oxygen.

3.3.2.4. DRIFTS analysis under the ethanol–water mixture Fig. 9 shows the DRIFTS spectra at different temperatures under the ethanol–water mixture. The assignments of the IR bands observed under the ethanol–water feed were similar to those obtained under the ethanol feed. Comparing the results with the spectrum obtained during the feeding of ethanol alone (Fig. 7) reveals significant differences in the relative band intensities. The ratio between the intensities of acetate species/ethoxy species and adsorbed CO/ethoxy species strongly increased in the presence of co-fed water. This finding suggests that water was somehow involved in the reaction scheme during the formation of acetate species; the mechanistic Scheme 3 is consistent with this.

When the sample was heated to 373 K, the intensities of the bands assigned to acetate species and to linearly adsorbed CO on Pt particles increased, whereas those of the bands of ethoxy species decreased. Adding water to the feed also promoted the formation of acetate species at this temperature, in agreement with an earlier study [20].

The spectrum at 473 K reveals the very strong intensities of the bands of acetate species and adsorbed CO. Gas-phase CO_2 was clearly detected at 573 K. At this temperature and above, it is obvious that the CO_2 production was in agreement with that shown in Scheme 4.

Above 673 K, the intensities of the bands characteristic of acetate species and adsorbed CO decreased significantly. Comparing the spectra of Figs. 7 and 9 shows that water likely promoted the acetate decomposition reaction (Scheme 5). The simultaneous formation of CO_2 and CH_4 is consistent with forward acetate decomposition to CO_2 and CH_4, as described in Schemes 4 and 5. This pathway would be favored when co-adsorbed H_2O is prevalent, as in the case of SR.

In light of this finding, and returning to the catalytic testing data, the initial deactivation rate of the catalyst was slower at higher H_2O/ethanol ratios. It is suggested that H_2O promotes the ethoxy → acetate → methane pathway, because higher initial methane selectivity occurs at higher H_2O/ethanol ratios. It was pointed out before that the deactivation of the catalyst to be asso-

ciated with a change in selectivity toward acetaldehyde production. This suggests that the turnover of ethoxy to acetate, which preceded demethanation, was increasingly hindered as a function of time on stream in favor of ethoxy dehydrogenation to acetaldehyde. Consistent with the slower initial deactivation rates observed at higher H_2O/ethanol ratios, the onset of the rise in acetaldehyde selectivity occurred at a later time on stream with increasing H_2O/ethanol ratio as well.

The literature contains many IR studies of adsorbed ethanol on different catalysts [5,13,14,16,18,46–48]. In general, ethanol or an ethanol–water mixture was adsorbed at room temperature, and then the evolution of species adsorbed on the surface during heating under vacuum was evaluated by IR analysis. Our results show that IR experiments under reaction conditions are fundamental to obtain reliable information that more closely reflects the reaction conditions of the true catalytic test.

4. Conclusions

In this work, catalytic performance parameters were explored to evaluate the ability of the $Pt/CeZrO_2$ catalyst to convert ethanol during several important hydrogen production reactions. At a lower operating temperature (773 K), the catalyst was found to deactivate significantly during ED and SR. Adding oxygen to the feed improved the catalyst stability from the standpoint of conversion; however, it also adversely affected hydrogen selectivity, as a significant fraction of the hydrogen product formed was in turn oxidized to water. For SR, increasing the water/ethanol ratio tended to favor the SR reaction route at the expense of catalyst stability. Increasing the reaction temperature from 773 to 1073 K greatly improved the catalyst stability. Thermodynamic calculations revealed that the product composition was closer to equilibrium.

DRIFTS was used to investigate the working reaction mechanisms under typical reaction conditions. Ethanol dissociatively adsorbs to generate ethoxy species and adsorbed H (as an –OH group). The catalytic decomposition of ethoxy species may follow different pathways: (i) decomposition to CO, CH_4, and H_2 or (ii) dehydrogenation to acetaldehyde and acetyl species. The dehydrogenated species may in turn undergo support-induced oxidation to acetate species, with either surface O^* or $–OH^*$ supplying the O required. As a result, adding co-fed water promoted acetate species formation. As an added benefit, water also aided the acetaldehyde and acetate decomposition reactions to methane, CO, and carbonate (i.e., forward decomposition). The formation rates of acetaldehyde and the oxidation of ethoxy species to acetate species were more significant during POX, in which the support may supply O^* directly (e.g., redox). Our IR experiments performed under actual reaction conditions provided critical information more relevant to the true catalytic test.

Acknowledgments

Financial support was provided by CNPq and CTENERG/FINEP (01.04.0525.00). CAER researchers acknowledge funding support from the Commonwealth of Kentucky.

References

[1] R.J. Farrauto, Appl. Catal. B 56 (2005) 3.
[2] R.M. Navarro, M.C. Alvarez-Galvan, M.C. Sanchez-Sanchez, F. Rosa, J.L.G. Fierro, Appl. Catal. B 55 (2004) 223.
[3] P.D. Vaidya, A.E. Rodrigues, Ind. Eng. Chem. Res. 45 (2006) 6614.
[4] A. Haryanto, S. Fernando, N. Murali, S. Adhikari, Energy Fuels 19 (2005) 2098.
[5] H. Song, L. Zhang, R.B. Watson, D. Braden, U.S. Ozkan, Catal. Today 129 (2007) 346.
[6] H. Roh, Y. Wang, D.L. King, A. Platon, Y. Chin, Catal. Lett. 108 (2006) 15.
[7] F. Romero-Sarria, J.C. Vargas, A. Roger, A. Kiennemann, Catal. Today 133 (2008) 149.
[8] F. Aupretre, C. Descorne, D. Duprez, Catal. Commun. 3 (2002) 263.
[9] C. Diagne, H. Idriss, A. Kiennemann, Catal. Commun. 3 (2002) 565.
[10] L.V. Mattos, F.B. Noronha, J. Power Sources 145 (2005) 10.
[11] S.M. de Lima, A.M. Silva, I.O. da Cruz, L.V. Mattos, F.B. Noronha, in: Proc. EUROPACAT VIII, CD ROM, paper P11_16, 2007.
[12] L.V. Mattos, F.B. Noronha, J. Power Sources 152 (2005) 50.
[13] L.V. Mattos, F.B. Noronha, J. Catal. 233 (2005) 453.
[14] A. Yee, S.J. Morrison, H. Idriss, J. Catal. 186 (1999) 279.
[15] P.-Y. Sheng, A. Yee, G.A. Bowmaker, H. Idriss, J. Catal. 208 (2002) 393.
[16] H. Idriss, C. Diagne, J.P. Hindermann, A. Kiennemann, M.A. Barteau, J. Catal. 155 (1995) 219.
[17] A. Erdohelyi, J. Raskó, T. Kecskés, M. Tóth, M. Dömök, K. Baán, Catal. Today 116 (2006) 367.
[18] M. Dömök, M. Tóth, J. Raskó, A. Erdohelyi, Appl. Catal. B 69 (2007) 262.
[19] C.E. Hori, H. Permana, K.Y. Ng Simon, A. Brenner, K. More, K.M. Rahmoeller, D. Belton, Appl. Catal. B 16 (1998) 105.
[20] G. Jacobs, R.A. Keogh, B.H. Davis, J. Catal. 245 (2007) 326.
[21] M. Boudart, Adv. Catal. 20 (1969) 153.
[22] P. Pantu, G.R. Gavalas, Appl. Catal. A 223 (2002) 253.
[23] S. Cavallaro, V. Chiodo, A. Vita, S. Freni, J. Power Sources 123 (2003) 10.
[24] F.B. Passos, E.R. de Oliveira, L.V. Mattos, F.B. Noronha, Catal. Today 101 (2005) 23.
[25] F. Fally, V. Perrichon, H. Vidal, J. Kaspar, G. Blanco, J.M. Pintado, S. Bernal, G. Colon, M. Daturi, J.C. Lavalley, Catal. Today 59 (2000) 373.
[26] D. Martine, D. Duprez, J. Phys. Chem. 100 (1996) 9429.
[27] S.H. Overbury, D.R. Huntley, D.R. Mullins, G.N. Glavee, Catal. Lett. 51 (1998) 133.
[28] J. Kugai, S. Velu, C. Song, Catal. Lett. 101 (2005) 255.
[29] H. Roh, A. Platon, Y. Wang, D.L. King, Catal. Lett. 110 (2006) 1.
[30] V. Fierro, O. Akidim, C. Mirodatos, Green Chem. 5 (2003) 20.
[31] A.N. Fatsikostas, D.I. Kondarides, X.E. Verykios, Catal. Today 75 (2002) 145.
[32] V. Klouz, V. Fierro, P. Denton, H. Katz, J.P. Lisse, S. Bouvot-Mauduit, C. Mirodatos, J. Power Source 105 (2002) 26.
[33] V. Fierro, V. Klouz, O. Akdim, C. Mirodatos, Catal. Today 75 (2002) 141.
[34] A.N. Fatsikostas, X.E. Verykios, J. Catal. 225 (2004) 439.
[35] A.F. Ghenciu, Curr. Opin. Solid State Mater. Sci. 6 (2002) 389.
[36] A.N. Fatsikostas, D.I. Kondarides, X.E. Verykios, Chem. Commun. (2001) 851.
[37] T. Montini, L. De Rogatis, V. Gombac, P. Fornasiero, M. Graziani, Appl. Catal. B 71 (2007) 125.
[38] E.Y. Garcia, M.A. Laborde, Int. J. Hydrogen Energy 16 (1991) 307.
[39] K. Vasudeva, N. Mitra, P. Umasankar, S.C. Dhingra, Int. J. Hydrogen Energy 21 (1996) 13.
[40] I. Fishtik, A. Alexander, R. Datta, D. Geana, Int. J. Hydrogen Energy 25 (2000) 31.
[41] A. Platon, H.S. Roh, D.L. King, Y. Wang, Top. Catal. 46 (2007) 374.
[42] M.A.S. Baldanza, L.F. de Mello, A. Vannice, F.B. Noronha, M. Schmal, J. Catal. 192 (2000) 64.
[43] E.M. Cordi, J.L. Falconer, J. Catal. 162 (1996) 104.
[44] L.F. de Mello, F.B. Noronha, M. Schmal, J. Catal. 220 (2003) 358.
[45] S.M. Stagg-Williams, F.B. Noronha, G. Fendley, D.E. Resasco, J. Catal. 194 (2000) 240.
[46] A. Yee, S.J. Morrison, H. Idriss, J. Catal. 191 (2000) 30.
[47] A. Yee, S.J. Morrison, H. Idriss, Catal. Today 63 (2000) 327.
[48] J. Rasko, A. Hancz, A. Erdohelyi, Appl. Catal. A 269 (2004) 13.
[49] C. Binet, M. Daturi, J.C. Lavalley, Catal. Today 50 (1999) 207.
[50] G. Jacobs, R.A. Keogh, B.H. Davis, Appl. Catal. A 285 (2005) 43.
[51] A.M. Silva, A.P.M.G. Barandas, L.O.O. Costa, L.E.P. Borges, L.V. Mattos, F.B. Noronha, Catal. Today 129 (2007) 297.
[52] P.V. Menacherry, G.L. Haller, J. Catal. 177 (1998) 175.
[53] H. Bischoff, N.I. Jaeger, G. Schulz-Ekloff, L. Kubelkova, J. Mol. Catal. 80 (1993) 95.
[54] M. Primet, J. Catal. 88 (1984) 273.
[55] R. Shekhar, M.A. Barteau, R.V. Plank, J.M. Vohs, J. Phys. Chem. B 101 (1997) 7939.
[56] T. Shido, Y. Iwasawa, J. Catal. 141 (1993) 71.